Modeling a Quadrotor Unmanned Aerial Vehicle and Robustness Analysis of Different Controller Designs under Parameter Uncertainty and Noise Disturbance

Mehmet Karahan, Cosku Kasnakoglu

Electrical and Electronics Engineering Department, TOBB University of Economics and Technology, Ankara 06510 Turkey (Tel: +90 (312) 292 4123; e-mail: m.karahan@etu.edu.tr, kasnakoglu@etu.edu.tr).

Abstract: Recent progresses in microelectromechanical system sensor technologies, energy storage devices, actuators and data processing enable development of micro unmanned aerial vehicles. This study gives information about modeling a micro vertical take-off landing unmanned aerial vehicle and robustness analysis of different controller designs. Different types of controllers developed for altitude and attitude control of an unmanned aerial vehicle. Altitude and attitude reference tracking performance of nonlinear controllers were analyzed. The effect of parameter uncertainty and noise disturbance on the reference tracking were also examined. Various simulations were performed under different conditions, and performance of the controllers compared with each other. Reference tracking performance and robustness analysis against parameter uncertainties and noise disturbance of controllers evaluated in the last section.

Keywords: Backstepping control, Lyapunov stability, Gaussian noise, parameter uncertainty, PID control, quadrotor, UAV.

1. INTRODUCTION

In the last decades, the quadrotor unmanned aerial vehicles (UAVs) have gained important research interest in both civilian and defense industry due to its basic structure, low-cost, vertical take-off and landing (VTOL) capability, as well as swift and secure maneuverability in dangerous missions. Quadrotors can complete diversified tasks such as aerial inspection, mapping, monitoring, crop spraying, cargo transport, search and rescue, border patrol and firefighting (Alexis et al., 2014; Da Silva Ferreira et al., 2020).

Boubdallah, Noth and Siegwart developed a test bench for 3 degrees of freedom (DOF) system, designed Proportional Integral Derivative (PID) and Linear Quadratic Regulator (LQR) control techniques for attitude control of quadrotor UAV. They neglected gyroscopic effects, they linearized rotor dynamics and neglected small coefficients of rotor dynamics. (Bouabdallah et al., 2004a). Mahony, Kumar and Corke developed Proportional Derivative (PD) controller for a quadrotor UAV (Mahony et al., 2012). Akgun et al. developed a Lyapunov-based model reference adaptive control of a quadrotor and ignored gyroscopic effects and friction forces at their dynamic model (Akgun, 2017). Wang et al. designed a fuzzy backstepping sliding mode controller for a tri-rotor unmanned aerial vehicle (Wang et al., 2017). Pei et al. proposed a vision based fuzzy controller for a target tracking system consists of a fixed-wing UAV with single-axis gimbal (Pei et al., 2018). Xiong and Zhang designed a sliding mode controller for position and attitude control of the quadrotor with parameter uncertainties (Xiong et al., 2016). Boudai et al. designed an adaptive control for a quadrotor UAV in the presence of Gaussian white noise and parameter uncertainties with respect to quadrotor mass and inertia matrix (Bouadi et al., 2015). Zhao et al. developed an active disturbance rejection switching control algorithm for trajectory tracking control of a quadrotor under noise disturbance (Zhao et al., 2020).

In this study, 6 DOF nonlinear model of a four-rotor micro UAV is presented. Gyroscopic effects, aerodynamic coefficients and small rotor dynamics are considered. None of the UAV parameters and coefficients have been ignored and none of the parameters and coefficients have been linearized. In this work, fixed axis gimbal was not used, therefore, altitude and attitude tracking could be observed through simulations. Enhanced PID controller, Lyapunov-based controller and backstepping controller are designed for the altitude and attitude control of the UAV. Parameter uncertainties and noise disturbance are applied to the UAV. Controllers' performances under normal conditions, under parameter uncertainties, under noise disturbance and under simultaneous parameter uncertainties and noise disturbance are examined through various simulations. MATLAB Simulink has been used to build quadrotor model and used to design controllers. It has also been used to compare the performances of the controllers against parameter uncertainties and noise. The contributions of this paper can be summarized as follows: First, the robustness of the Enhanced PID controller, Lyapunov-based controller and backstepping controller against parameter uncertainties are analyzed. Second, the performances of the Enhanced PID controller, Lyapunov-based controller and backstepping controller under noise are analyzed. Third, the robustness of the controllers is analyzed under simultaneous parameter uncertainties and noise disturbance.

The rest of this paper is organized as follows: In Sect. 2 the nonlinear model of quadrotor UAV is presented. In Sect. 3 controller designs are described. Altitude and attitude reference tracking simulations under parameter uncertainty and noise disturbance are examined in Sect. 4. Finally, conclusion of this study is given in Sect. 5.

2. THE QUADROTOR MODEL

Quadrotor UAV is propelled by four rotors. There are two types of the quadrotor configurations: plus type configuration and cross type configuration (Wang et al., 2016). In this work,

cross type configuration is preferred. In cross configuration, (1,3) and (2,4) rotor pairs turn in counter directions. Increasing or reducing all rotors' speeds together leads to vertical movement. Changing 1st and 3rd propellers' speed oppositely produces roll movement. Changing 2nd and 4th propellers' speed oppositely produces pitch movement. Counter torque between (1,3) and (2,4) pairs of propellers, generates yaw motion (Karahan et al., 2019; Bouabdallah et al., 2004b).

Quadrotor UAV's movements, angles, Body frame axis and Earth frame axis are shown in Fig.1.

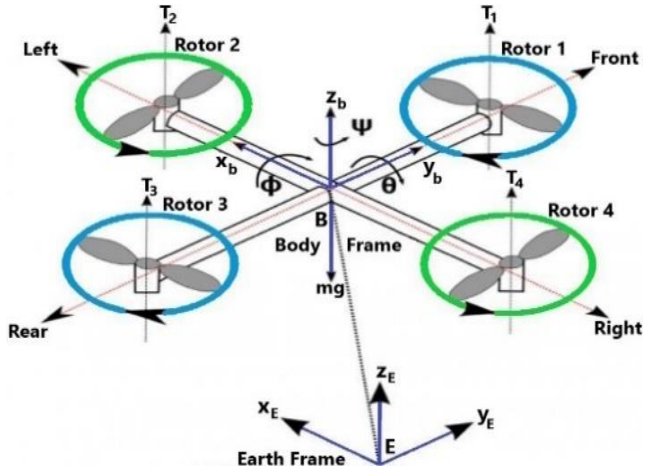

Fig. 1. Quadrotor model.

2.1 Quadrotor Kinematics and Dynamics

Rotation matrix is used for conversion from inertial centered frame to body centered frame. Equations (1-4) provide the conversion between earth centered frame and body centered frame (Da Silva Ferreira et al., 2020; Bresciani, 2008).

$$R(\psi) = \begin{bmatrix} \cos\psi & \sin\psi & 0 \\ -\sin\psi & \cos\psi & 0 \\ 0 & 0 & 1 \end{bmatrix} \quad (1)$$

$$R(\theta) = \begin{bmatrix} \cos\theta & 0 & -\sin\theta \\ 0 & 1 & 0 \\ \sin\theta & 0 & \cos\theta \end{bmatrix} \quad (2)$$

$$R(\varphi) = \begin{bmatrix} 1 & 0 & 0 \\ 0 & \cos\varphi & \sin\varphi \\ 0 & -\sin\varphi & \cos\varphi \end{bmatrix} \quad (3)$$

$$R(\varphi, \theta, \psi) = R(\varphi)\, R(\theta)\, R(\psi) \quad (4)$$

R represents orthogonal rotation matrix and it is given with Eq. 5 below. c and s represent cos and sin angles.

$$R = \begin{bmatrix} c\psi c\theta & s\psi c\theta & -s\theta \\ c\psi s\theta s\varphi - c\varphi s\psi & s\theta s\varphi s\psi + c\varphi c\psi & c\theta s\varphi \\ c\psi c\varphi s\theta + s\varphi s\psi & s\theta s\psi c\varphi - s\varphi c\psi & c\theta c\varphi \end{bmatrix} \quad (5)$$

Eq. 6 below indicates the transition from Euler angles to body axis rates. The Eq. 7 indicates the transition from body axis rates to Euler angles (Bresciani, 2008).

$$\begin{bmatrix} \dot{\Phi} \\ \dot{\theta} \\ \dot{\psi} \end{bmatrix} = \begin{bmatrix} 1 & \tan\theta \sin\varphi & \tan\theta \cos\varphi \\ 0 & \cos\varphi & -\sin\varphi \\ 0 & \sec\theta \sin\varphi & \sec\theta \cos\varphi \end{bmatrix} \begin{bmatrix} p \\ q \\ r \end{bmatrix} \quad (6)$$

$$\begin{bmatrix} p \\ q \\ r \end{bmatrix} = \begin{bmatrix} 1 & 0 & -\sin\theta \\ 0 & \cos\varphi & \cos\theta \sin\varphi \\ 0 & -\sin\varphi & \cos\theta \cos\varphi \end{bmatrix} \begin{bmatrix} \varphi' \\ \theta' \\ \psi' \end{bmatrix} \quad (7)$$

Let F_i indicate thrust and T_i indicate torque generated by ith rotor. Let w_i represent ith rotor's speed (i = 1 to 4). Let the constant b be thrust, d be drag coefficient and define $w_r = -w_1 + w_2 - w_3 + w_4$. Let l indicate quadrotor's arm length. One can then write (Bresciani, 2008; Dikmen et al., 2009).

$$F_i = b.w_i^2 \quad (8)$$

$$T_i = d.w_i^2 \quad (9)$$

The force equation and torque equation are given in Eq. 10 where U_1 represents force generated by all propellers; U_2, U_3 and U_4 are applied torques on quadrotor (Vaidyanathan et al., 2017). U_1, U_2, U_3 and U_4 represent control inputs and Eq. 10 gives control effectiveness equation.

$$u = \begin{bmatrix} U_1 \\ U_2 \\ U_3 \\ U_4 \end{bmatrix} = \begin{bmatrix} F \\ T_\varphi \\ T_\theta \\ T_\psi \end{bmatrix} = \begin{bmatrix} b & b & b & b \\ 0 & -lb & 0 & lb \\ lb & 0 & -lb & 0 \\ -d & d & -d & d \end{bmatrix} \begin{bmatrix} w_1^2 \\ w_2^2 \\ w_3^2 \\ w_4^2 \end{bmatrix} \quad (10)$$

Conversion from omega to force and torques is represented below in Eq. 11. (Vaidyanathan et al., 2017). Equation 11 represents inverse control effectiveness equation.

$$\begin{bmatrix} w_1^2 \\ w_2^2 \\ w_3^2 \\ w_4^2 \end{bmatrix} = \begin{bmatrix} \frac{1}{4b} & 0 & \frac{1}{2bl} & -\frac{1}{4d} \\ \frac{1}{4b} & -\frac{1}{2bl} & 0 & \frac{1}{4d} \\ \frac{1}{4b} & 0 & -\frac{1}{2bl} & -\frac{1}{4d} \\ \frac{1}{4b} & \frac{1}{2bl} & 0 & \frac{1}{4d} \end{bmatrix} \begin{bmatrix} U_1 \\ U_2 \\ U_3 \\ U_4 \end{bmatrix} \quad (11)$$

The complete mathematical model of the quadrotor due to translational and rotational motion is given in Eqs. (12) - (17) (Vaidyanathan et al., 2017; Eltayeb et al., 2020).

$$\ddot{X} = (\cos\varphi\cos\psi\sin\theta + \sin\varphi\sin\psi)\frac{U1}{m} \quad (12)$$

$$\ddot{Y} = (\cos\varphi\sin\psi\sin\theta - \sin\varphi\cos\psi)\frac{U1}{m} \quad (13)$$

$$\ddot{Z} = -g + (\cos\theta\cos\varphi)\frac{U1}{m} \quad (14)$$

$$\ddot{\varphi} = \dot{\theta}\dot{\psi}\left(\frac{I_y - I_z}{I_x}\right) + \dot{\theta} w_r \frac{J_R}{I_x} + \frac{l}{I_x} U_2 \quad (15)$$

$$\ddot{\theta} = \dot{\theta}\dot{\psi}\left(\frac{I_z - I_x}{I_y}\right) + \dot{\varphi} w_r \frac{J_R}{I_x} + \frac{l}{I_y} U_3 \quad (16)$$

$$\ddot{\psi} = \dot{\varphi}\dot{\theta}\left(\frac{I_x - I_y}{I_z}\right) + \frac{1}{I_z} U_4 \quad (17)$$

The OS4 quadrotor platform is used in this study. Table 1 represents the physical properties of the quadrotor (Vepa et al., 2016).

The inertia moments of the quadrotor can be calculated as below equations. M_{sphere} is the mass of the spherical dense center, r is the radius, M_{rotor} is the mass of the rotor and l is the quadrotor's arm length (Sanca et al., 2008).

Table 1. Quadrotor constants.

Constant	Definition	Value
m	Quadrotor mass	0.65 kg
l	Quadrotor arm length	0.23 m
g	Gravity	9.81m/s^2
b	Thrust coefficient	3.13x10^{-5} Ns^2
d	Drag coefficient	7.5x10^{-7} Ns^2
w_{max}	Maximum rotor speed	1000 rad/s
t_{max}	Maximum torque	0.15 Nm
Jr	Rotor Inertia	6.5x10^{-5} kgm^2
Ix	Inertia on x	7.5x10^{-3} kgm^2
Iy	Inertia on y	7.5x10^{-3} kgm^2
Iz	Inertia on z	1.3x10^{-2} kgm^2

$$I_x = \frac{2}{5} M_{sphere}\, r^2 + 2l^2\, M_{rotor} \quad (18)$$

$$I_y = \frac{2}{5} M_{sphere}\, r^2 + 2l^2\, M_{rotor} \quad (19)$$

$$I_z = \frac{2}{5} M_{sphere}\, r^2 + 4l^2\, M_{rotor} \quad (20)$$

Fig. 2 shows the schematic representation of spherical mass and point masses of mass M_{rotor} of the quadrotor.

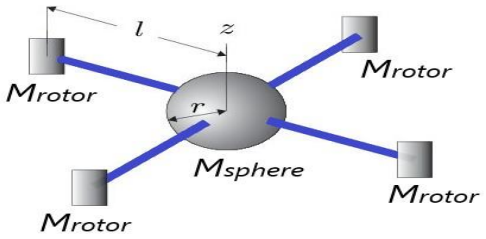

Fig. 2. The spherical mass and point masses.

3. CONTROLLER DESIGNS

In this section, three different types of controllers are designed for addressing the altitude and attitude control problem for the quadrotor UAV. Enhanced PID, Lyapunov-based and backstepping controllers are constructed with the aim of reference tracking under normal conditions, under parameter uncertainties, under noise disturbance and under simultaneous parameter uncertainities and noise disturbance.

3.1 Enhanced PID controller design

In this part, Enhanced PID controller is designed with the goal of controlling altitude and attitude of the quadrotor. In Enhanced PID controller, derivative gain is computed from output to avert keen motions because of the sudden impulse. In altitude reference and attitude angle controllers, a saturation block is added to get a more stable reference tracking. Saturation function bounds are between [-1,1]. The PID block scheme for altitude controller is given in the Fig. 3.

First, describe the altitude tracking error as:

$$e_z = z_d - z \quad (21)$$

z_d represents desired altitude. U_1 is control input of altitude controller and it is given in the Equation (22) (Jeong et al., 2016). θ angle represents rotation around y axis and φ angle represents rotation around x axis. During vertical flight, the quadrotor does not rotate in the x and y axes, so the denominator of the U_1 equation is never 0.

$$U_1 = \frac{\left(g + Kp.e_z + Ki\int e_z dt - Kd\frac{d}{dt}e_z\right).m}{cos\varphi cos\theta} \quad (22)$$

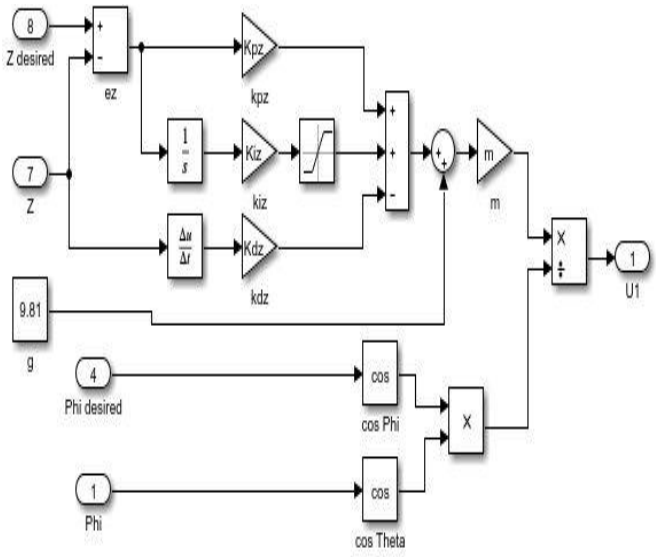

Fig. 3. The block diagram of the altitude controller.

In PID control approach, Kp, Ki, and Kd are constants of the controller. Proportional parameter Kp decreases rise time but it leads to overshoot. Because of this, derivative parameter Kd is used for decreasing overshoot and integral parameter Ki is set to reduce steady state error (Gautam et al., 2013; Dong et al., 2015). Table 2 lists the Enhanced PID parameters of the altitude controller.

The ITAE (integral of time weighted absolute error) criterion is used to tune PID parameters of altitude and attitude controllers. In this method, integral of time weighted absolute error is minimized to obtain a good performance. The ITAE performance index is mathemtically given in Equation (23).

$$\text{ITAE} = \int_0^\infty t|e(t)|dt \quad (23)$$

In Equation (23), t represents time and e(t) represents the difference between set point and controlled variable.

Table 2. PID parameters for altitude control.

Parameter	Value
Kp	0.835
Ki	0.103
Kd	1.665

Roll tracking error is defined in Equation (24) and U_2 control input for roll angle is given in Equation (25).

$$e_\varphi = \varphi_d - \varphi \quad (24)$$

$$U_2 = Kpe_\varphi + sat\, Ki\int e_\varphi\, dt - Kd\frac{d}{dt}\varphi \quad (25)$$

Pitch tracking error is defined in Equation (26) and U_3 control input for pitch angle is described in Equation (27).

$$e_\theta = \theta_d - \theta \tag{26}$$

$$U_3 = Kpe_\theta + sat\ Ki \int e_\theta\, dt - Kd \frac{d}{dt}\theta \tag{27}$$

Yaw tracking error is shown in Equation (28) and U_4 control input for yaw angle is represented in Eqaution (29).

$$e_\psi = \psi_d - \psi \tag{28}$$

$$U_4 = Kpe_\psi + sat\ Ki \int e_\psi\, dt - Kd \frac{d}{dt}\psi \tag{29}$$

Fig. 4. gives the PID control block scheme for roll control. Pitch and yaw control block diagrams are similar except for reference angles.

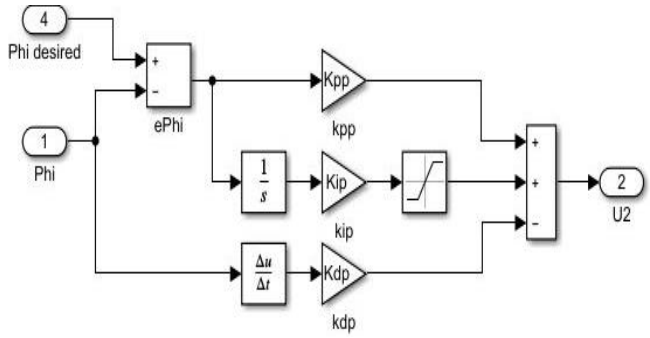

Fig. 4. The block diagram of the roll controller.

Table 3 presents Enhanced PID parameters for the attitude controllers.

Table 3. PID parameters for attitude controllers.

Parameter	Roll	Pitch	Yaw
Kp	0.116	0.134	0.127
Ki	0.045	0.065	0.043
Kd	0.054	0.073	0.092

3.2 Lyapunov-based controller design

Lyapunov stability theorem-based controller aims directly to control the position of the quadrotor. Let x = 0 be the equilibrium point. x = 0 is a globally asymptotically stable equilibrium point of the system and there exists a quadratic Lyapunov function. Assume that D is a compact neighborhood of f(0) in Rn. Rn is the coordinate space over the real numbers. R+ is the positive real numbers. Let the Lyapunov function V: D → R+ be a continuous function satisfying (Anderson et al., 2015; Jammazi et al., 2008; Flores et al., 2020).

$$V(0) = 0,\ V(x) > 0 \text{ in } D,\ x \neq 0 \tag{30}$$

$$\dot{V}(x) \leq 0 \text{ in } D \tag{31}$$

Then the equilibrium is stable in D domain. In the case of the equilibrium is asymptotically stable in D domain as shown in Equation 32 (Yigit, 2015).

$$\dot{V}(x) < 0 \text{ in } D,\ x \neq 0 \tag{32}$$

First a section is defined that contains stabilization angles and time derivates of them as desired position at equilibrium point of quadrotor for attitude control. For instance, X = (φ_d, 0, θ_d, 0, ψ_d, 0) where φ_d, θ_d and ψ_d, are desired roll, pitch and yaw angles. Their angular velocities and their time derivatives will be zero at the stabilization point (Yigit, 2015). Let

$$V(x) = \frac{1}{2}[\,(\varphi - \varphi_d)^2 + \dot{\varphi}^2 + (\theta - \theta_d)^2 + \dot{\theta}^2 + (\psi - \psi_d)^2 + \dot{\psi}^2\,] \tag{33}$$

V(x) is a positive defined Lyapunov function around the desired position. The derivative is given in Eq. 34.

$$\dot{V}(x) = (\varphi - \varphi_d)\,\dot{\varphi} + \dot{\varphi}\ddot{\varphi}_d + (\theta - \theta_d)\,\dot{\theta} + \dot{\theta}\ddot{\theta}_d + (\psi - \psi_d)\dot{\psi} + \dot{\psi}\ddot{\psi}_d \tag{34}$$

The function of angle and position given in Eqs. (12-17) could be simplified in the event of perfect cross VTOL (Ix=Iy). When the system near to the equilibrium point $w_r = 0$, $\dot{\varphi} = 0$, $\dot{\theta} = 0$, $\dot{\psi} = 0$ we get the equation below (Bouabdallah, 2007).

$$\dot{V}(x) = (\varphi - \varphi_d)\,\dot{\varphi} + \dot{\varphi}\frac{l}{Ix}U_2 + (\theta - \theta_d)\,\dot{\theta} + \dot{\theta}\frac{l}{Iy}U_3 + (\psi - \psi_d)\dot{\psi} + \dot{\psi}\frac{l}{Iz}U_4 \tag{35}$$

Then the control inputs are selected as below for stability.

$$U_2 = -\frac{Ix}{l}(\varphi - \varphi_d) - k_1\dot{\varphi} \tag{36}$$

$$U_3 = -\frac{Iy}{l}(\theta - \theta_d) - k_2\dot{\theta} \tag{37}$$

$$U_4 = -I_z(\psi - \psi_d) - k_3\dot{\psi} \tag{38}$$

In this case Eq. 35 becomes,

$$\dot{V}(x) = -\dot{\varphi}^2\frac{l}{Ix}k_1 - \dot{\theta}^2\frac{l}{Iy}k_2 - \dot{\psi}^2\frac{l}{Iz}k_3 \tag{39}$$

where k_1, k_2, k_3 coefficients are positive parameters described by Eqs. (36-39). The above function is negative semi-definite. The Lyapunov function and its derivative with respect to angles and altitude given in Eqs. (40-41) for altitude controller is,

$$V(x) = \frac{1}{2}[\,(z - z_d)^2 + \dot{z}^2\,] \tag{40}$$

$$\dot{V}(x) = (z - zd)\,\dot{z} + \dot{z}(g - (\cos\theta\cos\varphi)U_1/m) \tag{41}$$

U_1 control input is selected as below for stability.

$$U_1 = -\frac{m}{\cos\theta\cos\varphi}(z_d - z - g) - k_z\dot{z} \tag{42}$$

Then Eq. 41 becomes,

$$\dot{V}(x) = -\dot{z}^2 k_z \tag{43}$$

where k_z is a positive constant described by Eq. (43). The above function is negative semidefinite. Lyapunov-based controller's coefficients are shown in Table 4. k_1, k_2 and k_3 are attitude controller coefficients and k_z is the altitude coefficient.

Table 4. Lyapunov-based controller coefficients.

Parameter	Value
k_1	0.03
k_2	0.025
k_3	0.023
k_4	3.9

3.3 Backstepping controller design

Backstepping is a control technique used for nonlinear systems. Backstepping control relies on defining virtual control inputs which finally connect to the real input. First, a Lyapunov function in the tracking error z_1 is defined as positive-definite, and its time derivative is made negative semi-definite (Oland et al., 2013; Zhou et al., 2019). Let this tracking error be described as below:

$$z_1 = \varphi_d - \varphi \tag{44}$$

Lyapunov function and its time derivative are given as below (Liu et al., 2019; Lee et al., 2017).

$$V(z_1) = \frac{1}{2} z_1^2 \tag{45}$$

$$\dot{V}(z_1) = z_1(\dot{\varphi}_d - \dot{\varphi}) \tag{46}$$

A new virtual control input $\dot{\varphi}$ is used for the stabilization of z_1 function:

$$\dot{\varphi} = \dot{\varphi}_d + a_1 z_1 \tag{47}$$

a_1 should be a positive coefficient to obtain negative semi-definitiveness (Rui et al., 2017). When the virtual control input is defined as in Eq. 47, we obtain

$$\dot{V}(z_1) = - a_1 z_1^2 \tag{48}$$

Another variable change is as below:

$$z_2 = \dot{\varphi} - \dot{\varphi}_d - a_1 z_1 \tag{49}$$

The augmented Lyapunov function could then be defined as below (Meng et al., 2020).

$$V(z_1, z_2) = \frac{1}{2} z_1^2 + \frac{1}{2} z_2^2 \tag{50}$$

The Lyapunov function's time derivative is as follow:

$$\dot{V}(z_1, z_2) = - a_1 z_1^2 - z_1 z_2 + z_2 \ddot{\varphi} - z_2(\ddot{\varphi}_d - a_1(z_2 + a_1 z_1)) \tag{51}$$

According to Eq. 15, $\ddot{\varphi}$ variable could be rewritten as below:

$$\ddot{\varphi} = \dot{\psi}\dot{\theta} a_1 + a_2 \dot{\theta} w_r + \frac{l}{Ix} U_2 \tag{52}$$

The control input U_2 is defined as below under $\dot{\varphi}$, $\ddot{\varphi}$, $\ddot{\theta}_d = 0$ and $\dot{V}(z_1, z_2) < 0$ condition.

$$U_2 = \frac{Ix}{l}(z_1 - a_1 \dot{\theta}\dot{\psi} - a_2 \dot{\theta} \Omega_r - a_1(z_2 + a_1 z_1) - a_2 z_2) \tag{53}$$

In order to stabilize z_1, $a_2 z_2$ term with $a_2 > 0$ is added. Using the same idea, U_3 and U_4 control inputs which control pitch angle and yaw angle are extracted as below:

$$U_3 = \frac{Iy}{l}(z_3 - a_3 \dot{\varphi}\dot{\psi} - a_4 \dot{\varphi} \Omega_r - a_3(z_4 + a_3 z_3) - a_4 z_4) \tag{54}$$

$$U_4 = \frac{Iz}{1}(z_5 - a_5 \dot{\varphi}\dot{\theta} - a_5(z_6 + a_5 z_5) - a_6 z_6) \tag{55}$$

The definitions below are used in U_3 and U_4 control inputs:

$$z_3 = \theta_d - \theta \tag{56}$$

$$z_4 = \dot{\theta} - \dot{\theta}_d - a_3 z_3 \tag{57}$$

$$z_5 = \psi_d - \psi \tag{58}$$

$$z_6 = \dot{\psi} - \dot{\psi}_d - a_5 z_5 \tag{59}$$

The tracking error z_7 is defined for altitude control.

$$z_7 = z - z_d \tag{60}$$

$$V(z_7) = \frac{1}{2} z_7^2 \tag{61}$$

The Lyapunov function's time derivative is described as below:

$$\dot{V}(z_7) = z_7 (\dot{z}_d - \dot{z}) \tag{62}$$

The virtual control input x_8 is defined to stabilize the $\dot{V}(z_7)$ function.

$$x_8 = \dot{z}_d + a_7 z_7 \tag{63}$$

The second variable change is as below:

$$z_8 = x_8 - \dot{z}_d - a_7 z_7 \tag{64}$$

The new Lyapunov function of desired variables could be described as follows:

$$V(z_7, z_8) = \frac{1}{2} z_7^2 + \frac{1}{2} z_8^2 \tag{65}$$

This function's time derivative is,

$$\dot{V}(z_7, z_8) = - a_7 z_7^2 - z_7 z_8 + z_8 x_8 - z_8(\ddot{z}_d - a_7(z_8 + a_7 z_7)) \tag{66}$$

$$\dot{x}_8 = g - \cos\theta\cos\varphi \frac{U_1}{m} \tag{67}$$

$$U_1 = \frac{m}{\cos\theta\cos\varphi}(z_7 + g - a_7 (z_8 + a_7 z_7) - a_8 z_8) \tag{68}$$

Backstepping controller's coefficients are shown in Table 5.

Table 5. Backstepping controller coefficients

Coefficient	Roll (a1, a2)	Pitch (a3, a4)	Yaw (a5,a6)	Altitude (a7, a8)
a	(8.7, 7)	(8, 4)	(8.45, 4.05)	(1.5, 6)

4. SIMULATIONS

In this section, simulations of different types of controllers are presented. Enhanced PID, Lyapunov-based and backstepping controllers are compared with in terms of reference tracking under normal conditions, reference tracking under parameter uncertainties, reference tracking under noise disturbance and reference tracking under simultaneous parameter uncertainties and noise disturbance. The system was implemented in MATLAB Simulink. The block diagram of system is given in the Fig. 5. φ_d, θ_d and ψ_d, are desired roll, pitch and yaw trjectories. φ, θ and ψ are actual trajectories of quadrotor. U_1, U_2, U_3 and U_4 are control inputs.

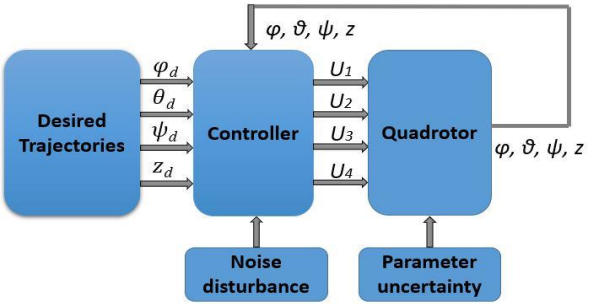

Fig. 5. The block diagram of the system.

4.1 Altitude and attitude reference tracking without parameter uncertainties and noise disturbance

Reference tracking comparison results under normal conditions are presented in Fig. 6 through Fig. 9. Rise time, overshoot and settling time comparison of Enhanced PID, Lyapunov-based and backstepping controllers under normal conditions are shown in Table 6. Rise time and settling time are in terms of seconds and overshoot is in terms of percent. Settling time is defined as the time required for the response curve to reach and stay within 2% of the final value. In Simulink, Bilevel Measurements panel is used to calculate rise time, overshoot and settling time values.

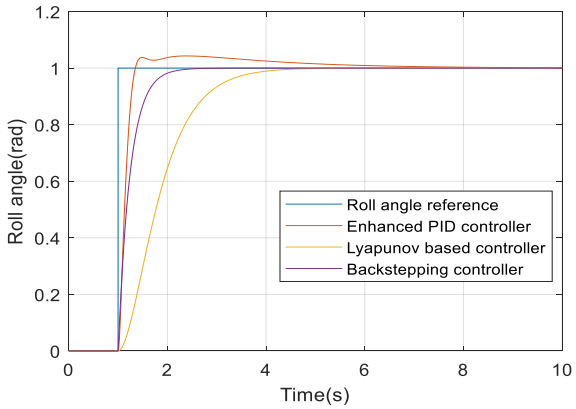

Fig. 6. Roll angle tracking under normal conditions.

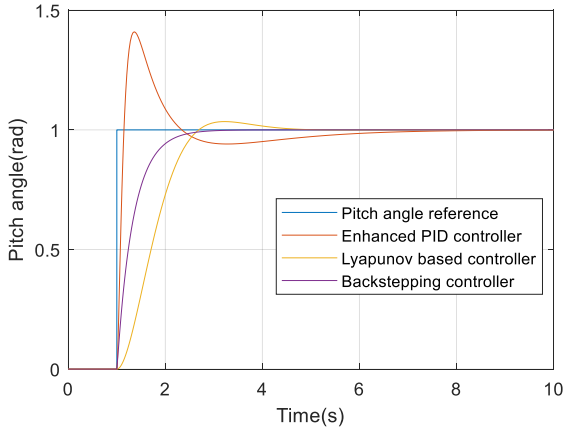

Fig. 7. Pitch angle tracking under normal conditions.

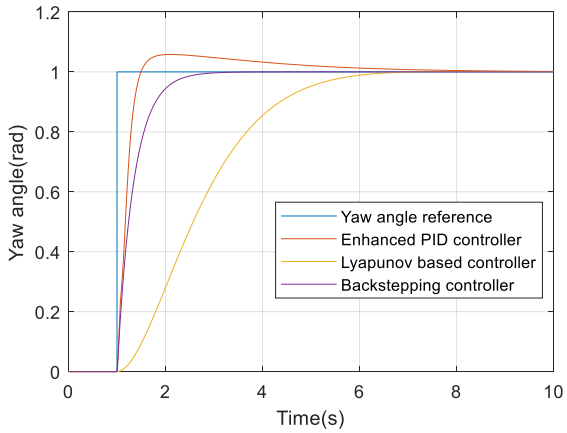

Fig. 8. Yaw angle tracking under normal conditions.

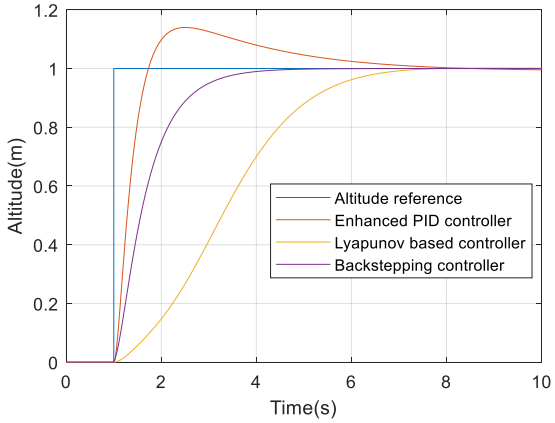

Fig. 9. Altitude tracking under normal conditions.

The backstepping controller appears to be superior to other two. It has a lower settling time than Enhanced PID and Lyapunov-based controllers. Backstepping controller does not exhibit overshoot while Enhanced PID controller prominently exhibits overshoot during reference tracking. Although the Enhanced PID controller has a fast rise time, it shows the highest overshoot value, and the settling time is long. Lyapunov-based controller also shows overshoot in pitch angle and roll angle reference tracking as shown in Table 6.

Table 6. Rise time, overshoot and settling time comparison of controllers under normal conditions.

Controller Type	Rise Time (s)	Overshoot (%)	Settling Time (s)
Roll angle Enhanced PID controller	0.23	3.12	4.53
Roll angle Lyapunov based controller	1.487	0.5	3.66
Roll angle Backstepping controller	0.52	0.49	1.99
Pitch angle Enhanced PID controller	0.1	42.14	5.47
Pitch angle Lyapunov based controller	1.06	3.64	3.82
Pitch angle Backstepping controller	0.75	0.5	2.45
Yaw angle Enhanced PID controller	0.32	5.85	5.13
Yaw angle Lyapunov based controller	2.8	-	5.66
Yaw angle Backstepping controller	0.74	0.5	2.38
Altitude Enhanced PID controller	0.49	14.37	6.68
Altitude Lyapunov based controller	4.85	-	6.43
Altitude Backstepping controller	1.39	0.5	3.62

4.2 Altitude and attitude reference tracking under parameter uncertainties

Next, +50% parameter uncertainty is applied to m, l, b, d, w_{max}, Jr, Ix, Iy and Iz parameters of the quadrotor. Simulation results

of Enhanced PID, Lyapunov-based and Backstepping controllers under +50% parameter uncertainties are presented in Fig. 10 through Fig. 13. It appears that the backstepping controller is more robust than Enhanced PID and Lyapunov-based controllers under +50% parameter uncertainties. Backstepping controller exhibits the shortest settling time without experiencing overshoot. Enhanced PID and Lyapunov-based controllers have longer settling time and higher overshoot as compared to the backstepping controller. While Enhanced PID controller has the shortest rise time amongst all controllers, it has the highest overshoot value and takes more time to reach the reference value than the backstepping controller

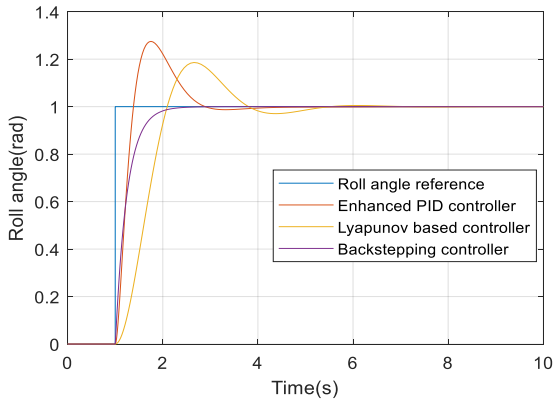

Fig. 10. Roll angle tracking under +50% parameter uncertainties.

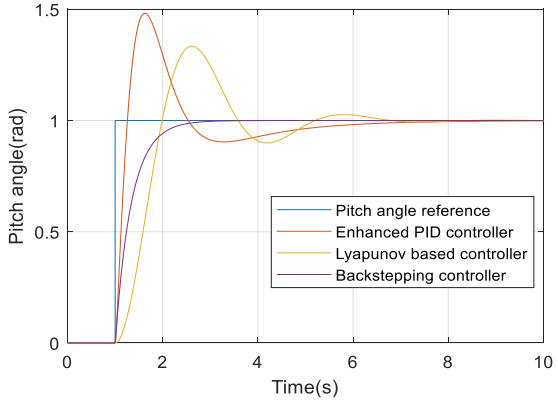

Fig. 11. Pitch angle tracking under +50% parameter uncertainties.

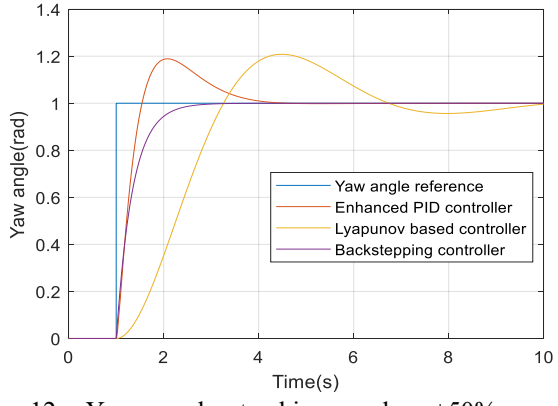

Fig. 12. Yaw angle tracking under +50% parameter uncertainties.

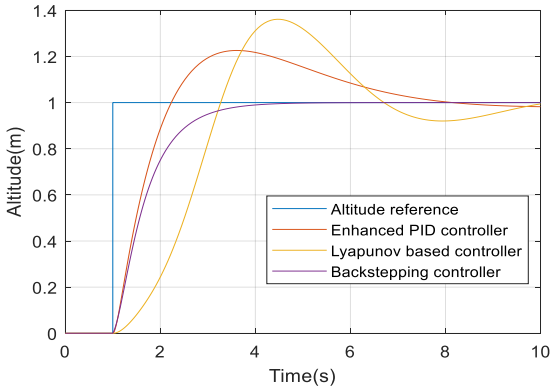

Fig. 13. Altitude tracking under +50% parameter uncertainties.

Rise time, overshoot and settling time comparison of Enhanced PID, Lyapunov-based and backstepping controllers under +50% parameter uncertainties are shown in Table 7.

Table 7. Rise time, overshoot and settling time comparison of controllers under +50% parameter uncertainties

Controller Type	Rise Time (s)	Overshoot (%)	Settling Time (s)
Roll angle Enhanced PID controller	0.27	27.6	2.91
Roll angle Lyapunov based controller	0.73	18.4	4.87
Roll angle Backstepping controller	0.53	0.49	1.95
Pitch angle Enhanced PID controller	0.19	48.5	6.03
Pitch angle Lyapunov based controller	0.66	34.5	6.19
Pitch angle Backstepping controller	0.75	0.5	2.41
Yaw angle Enhanced PID controller	0.39	18.5	3.8
Yaw angle Lyapunov based controller	1.45	25.9	9.33
Yaw angle Backstepping controller	0.74	0.5	2.42
Altitude Enhanced PID controller	0.87	24.38	7.52
Altitude Lyapunov based controller	1.44	48.5	9.66
Altitude Backstepping controller	1.39	0.5	3.69

Secondly, -50% parameter uncertainty is applied to parameters of the quadrotor. Enhanced PID, Lyapunov-based and backstepping controllers under -50% parameter uncertainties are presented in Fig. 14 through Fig. 17. It is obvious that the backstepping controller is more robust than Enhanced PID and Lyapunov-based controllers under -50% parameter uncertainties. It has the shortest settling time amongst all controllers as also shown in Table 8. Backstepping controller also exhibits very small overshoot values of around 0.5%. Enhanced PID and Lyapunov-based controllers have longer settling time as compared to the backstepping controller. Enhanced PID controller shows the highest overshoot values

as shown in Table 8. Lyapunov-based controller has the longest settling time, although it does not show overshoot.

Rise time, overshoot and settling time comparison of Enhanced PID, Lyapunov-based and backstepping controllers under -50% parameter uncertainties are shown in Table 8.

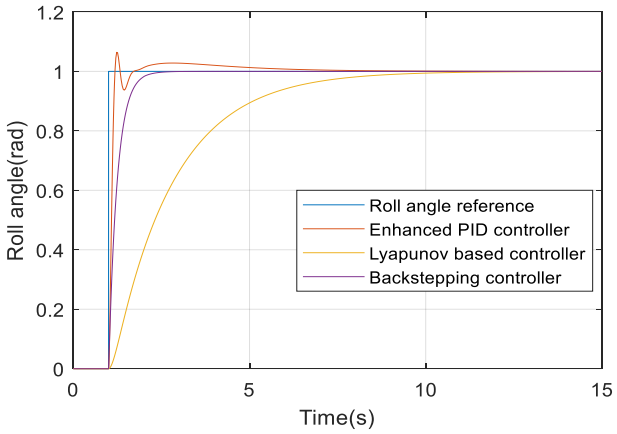

Fig. 14. Roll angle tracking under -50% parameter uncertainties.

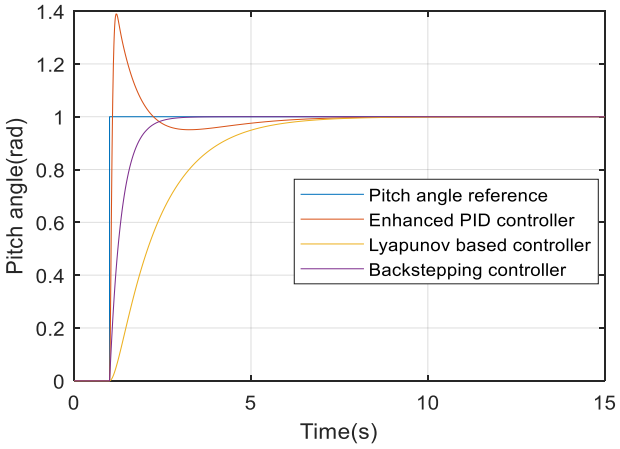

Fig. 15. Pitch angle tracking under -50% parameter uncertainties.

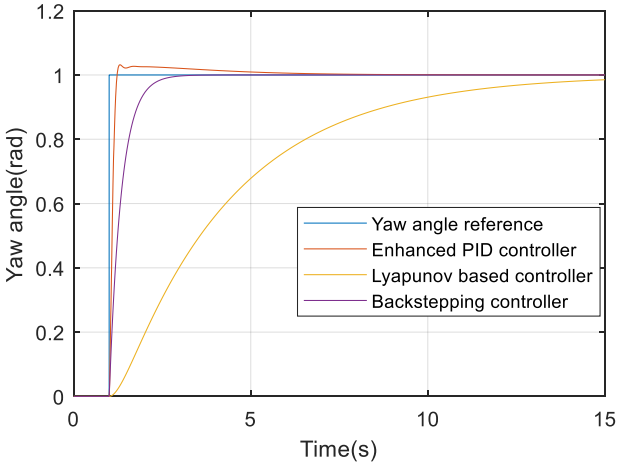

Fig. 16. Yaw angle tracking under -50% parameter uncertainties.

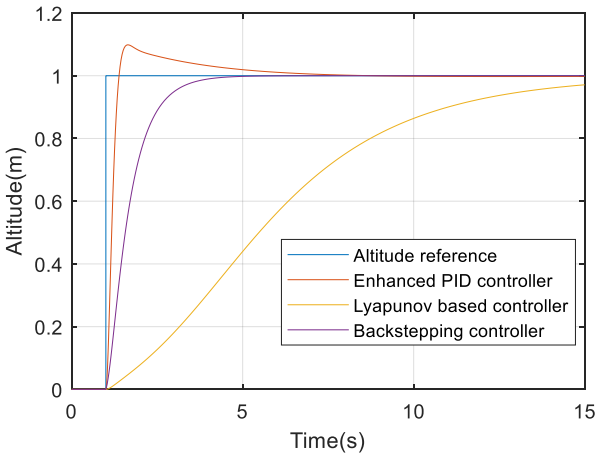

Fig. 17. Altitude tracking under -50% parameter uncertainties.

Table 8. Rise time, overshoot and settling time comparison of controllers under -50% parameter uncertainties.

Controller Type	Rise Time (s)	Overshoot (%)	Settling Time (s)
Roll angle Enhanced PID controller	0.12	5.86	4.45
Roll angle Lyapunov based controller	4.93	-	7.98
Roll angle Backstepping controller	0.53	0.49	1.99
Pitch angle Enhanced PID controller	0.57	40.14	5.5
Pitch angle Lyapunov based controller	4.15	-	6.36
Pitch angle Backstepping controller	0.75	0.5	2.42
Yaw angle Enhanced PID controller	0.15	2.57	3.74
Yaw angle Lyapunov based controller	8.67	-	14.1
Yaw angle Backstepping controller	0.74	0.5	2.41
Altitude Enhanced PID controller	0.25	10.55	5.21
Altitude Lyapunov based controller	10.89	-	15.78
Altitude Backstepping controller	1.39	0.5	3.68

4.3 Altitude and attitude reference tracking under noise disturbance

Next, band limited Gaussian white noise is imposed on the system. Simulations under noise are given below in Fig. 18 through Fig. 21. It is evident that the backstepping controller is more robust against Gaussian noise as compared to Enhanced PID and Lyapunov-based controllers. Backstepping controller has the shortest settling time. While Enhanced PID and Lyapunov-based controllers exhibit significant overshoot,

backstepping controller nearly does not show overshoot. It may be concluded that the backstepping controller can track altitude and attitude references better than Enhanced PID and Lyapunov-based controllers. Enhanced PID and Lyapunov-based controllers do not have a settling time for roll, pitch and yaw angle references because they could not reach and stay within 2% of the final reference value.

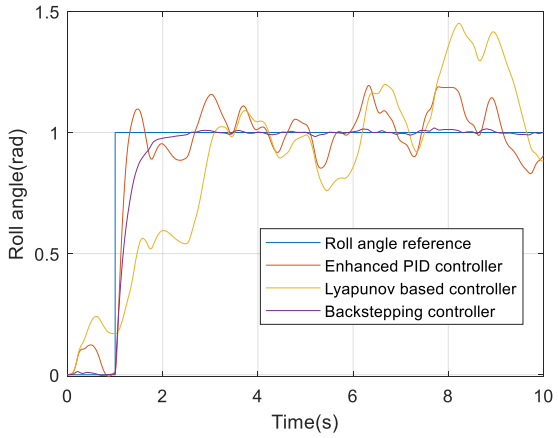

Fig. 18. Roll angle tracking under noise disturbance.

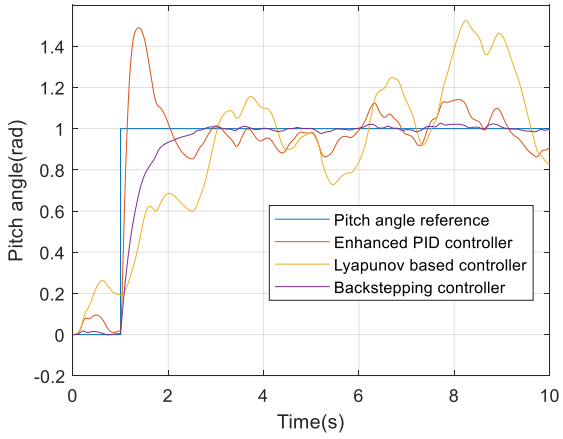

Fig. 19. Pitch angle tracking under noise disturbance.

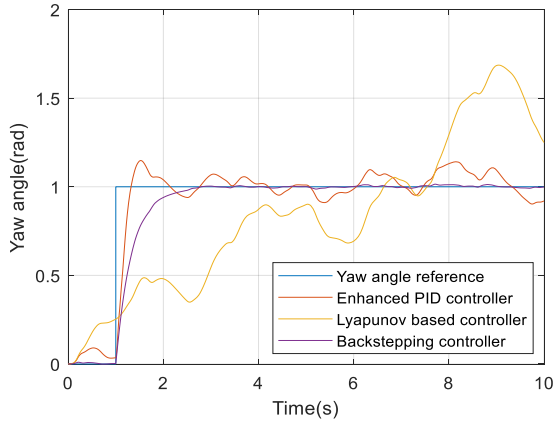

Fig. 20. Yaw angle tracking under noise disturbance.

Rise time, overshoot and settling time comparison of Enhanced PID, Lyapunov-based and backstepping controllers under noise disturbance are shown in Table 9.

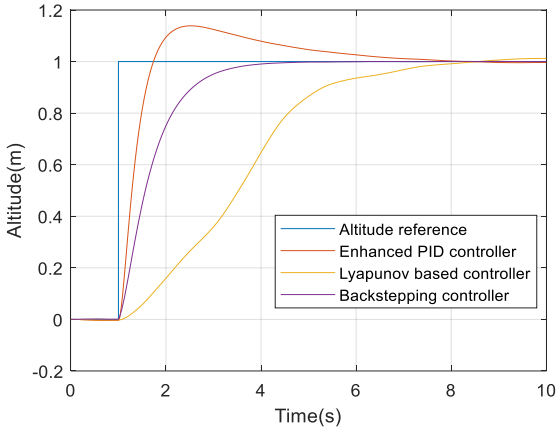

Fig. 21. Altitude tracking under noise disturbance.

Table 9. Rise time, overshoot and settling time comparison of controllers under noise disturbance

Controller Type	Rise Time (s)	Overshoot (%)	Settling Time (s)
Roll angle Enhanced PID controller	0.19	15.85	-
Roll angle Lyapunov based controller	1.83	45.08	-
Roll angle Backstepping controller	0.57	0.58	2.13
Pitch angle Enhanced PID controller	0.1	47.01	-
Pitch angle Lyapunov based controller	1.73	67.48	-
Pitch angle Backstepping controller	0.77	1.09	2.56
Yaw angle Enhanced PID controller	0.25	10.92	-
Yaw angle Lyapunov based controller	0.73	13.43	-
Yaw angle Backstepping controller	0.76	0.7	2.53
Altitude Enhanced PID controller	0.49	14.37	6.44
Altitude Lyapunov based controller	4.3	1.53	7.38
Altitude Backstepping controller	1.39	0.45	3.6

4.4 Altitude and attitude reference tracking under parameter uncertainties and noise disturbance

In this section, parameter uncertainties and noise disturbance are simultaneously imposed on the system. Simulations under parameter uncertainties and noise disturbance are given in Fig. 22 through Fig. 25. Backstepping controller shows the highest robustness to simultaneous parameter uncertainty and noise disturbance amongst all controllers. It has the shortest settling time. It can successfully track given references without overshoot. Enhanced PID and Lyapunov-based controllers do not have a settling time for roll, pitch and yaw angle referencesbecause they could not reach and stay within 2% of

the final reference value. Enhanced PID and Lyapunov-based controllers can only reach and stay within 2% of the altitude reference but it takes longer time than backstepping controller.

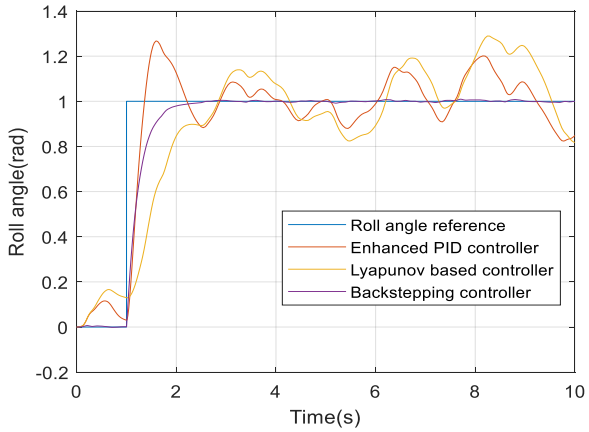

Fig. 22. Roll angle tracking under parameter uncertainties and noise disturbance.

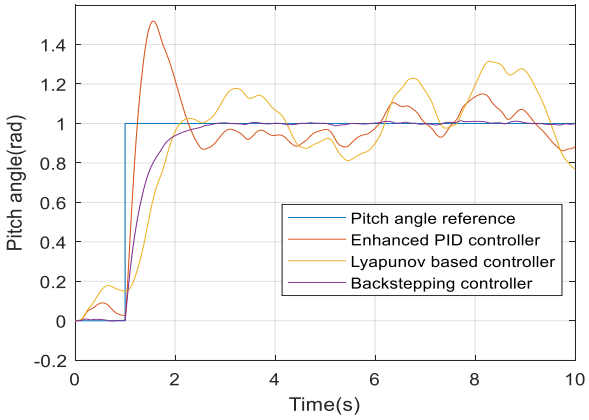

Fig. 23. Pitch angle tracking under parameter uncertainties and noise disturbance.

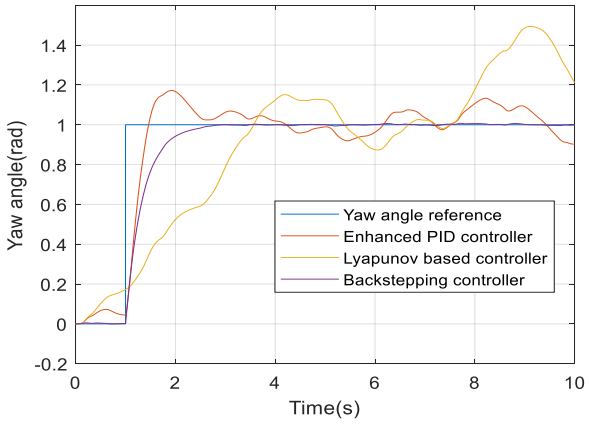

Fig. 24. Yaw angle tracking under parameter uncertainties and noise disturbance.

Rise time, overshoot and settling time comparison of Enhanced PID, Lyapunov-based and backstepping controllers under parameter uncertainties and noise disturbance are shown in Table 10.

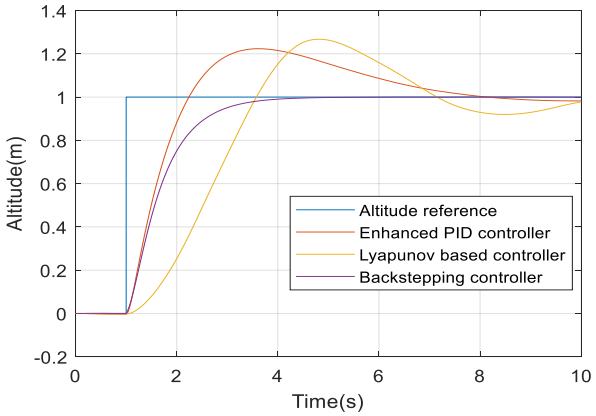

Fig. 25 Altitude tracking under parameter uncertainties and noise disturbance.

Table 10. Rise time, overshoot and settling time comparison of controllers under parameter uncertainties noise disturbance.

Controller Type	Rise Time (s)	Overshoot (%)	Settling Time (s)
Roll angle Enhanced PID controller	0.3	13.37	-
Roll angle Lyapunov based controller	0.67	41.6	-
Roll angle Backstepping controller	0.56	0.01	2.02
Pitch angle Enhanced PID controller	0.24	24.68	-
Pitch angle Lyapunov based controller	0.66	27.95	-
Pitch angle Backstepping controller	0.76	0.77	2.50
Yaw angle Enhanced PID controller	0.45	0.52	-
Yaw angle Lyapunov based controller	2.22	38.28	-
Yaw angle Backstepping controller	0.77	0.07	2.49
Altitude Enhanced PID controller	0.73	24.38	7.56
Altitude Lyapunov based controller	1.64	25.95	9.97
Altitude Backstepping controller	1.39	0.47	3.53

5. CONCLUSIONS

In this paper, Enhanced PID control, Lyapunov-based control and backstepping control strategies are proposed with the aim of reference tracking, as well as robustness to parameter uncertainties and noise disturbance.

First, a 6 DOF mathematical model of the quadrotor is set up based on Newton-Euler equations. Enhanced PID, Lyapunov-based and backstepping controllers are designed for altitude and attitude control of the quadrotor. Parameter uncertainties

and band-limited Gaussian white noise are applied to the quadrotor. The performances of the controllers were examined under four different conditions: under normal conditions, under parameter uncertainty, under noise, and under simultaneous parameter uncertainty and noise. Simulation results show that nonlinear backstepping controller achieves the best performance for reference tracking under normal conditions. Backstepping controller has also the best performance under parameter uncertainties and Gaussian white noise. While Lyapunov-based controller accomplishes reference tracking better than Enhanced PID controller, Enhanced PID controller seems more robust to parameter uncertainties and noise disturbance. To sum up, the simulation results stress that the nonlinear backstepping controller design used in this study shows an apparently improved performance than Enhanced PID and Lyapunov-based controller designs both in terms of reference tracking accuracy and robustness against parameter uncertainty and noise disturbance.

REFERENCES

Akgun, O., Subasi, E., and Turker, T. A. (2017). Lyapunov based model reference adaptive control of a quadrotor, *2017 10th International Conference on Electrical and Electronics Engineering (ELECO)*, 732-736.

Alexis, K., Nikolakopoulos, G., and Tzes, A. (2014). Experimental constrained optimal attitude control of a quadrotor subject to wind disturbances. *International Journal of Control, Automation and Systems,* 12(6), 1289–1302.

Ammar, N.B., Bouallègue, S., Haggège, J., Vaidyanathan, S. (2017). Chattering Free Sliding Mode Controller Design for a Quadrotor Unmanned Aerial Vehicle. Vaidyanathan, S., Lien, C.H. (ed.1) *Applications of Sliding Mode Control in Science and Engineering (Studies in Computational Intelligence Book 709)*, 61-79. Springer, New York.

Anderson, J., Papachristodoulou, A. (2015). Advances in Computational Lyapunov Analysis using sum-of-squares programming, *Discrete & Continuous Dynamical Systems - B*, 20(8), 2361-2381.

Bouabdallah, S., Noth, A., Siegwart, R. (2004). PID vs. LQ control techniques applied to an indoor micro quadrotor, *Proc. IEEE/RSJ Int. Conf. Intell. Robots Syst*., 3, 2451–2456.

Bouabdallah, S., Murrieri, P., Siegwart, R. (2004). Design and control of an indoor micro quadrotor, *IEEE International Conference on Robotics and Automation*, 4393–4398.

Bouabdallah, S. (2007). *Design and control of quadrotors with application to autonomous flying*, PhD Thesis, Ecole Polytechnical Federal Lausanne, Switzerland.

Liu, J., Gai, W., Zhang, J., Li, Y. (2019). Nonlinear Adaptive Backstepping with ESO for the Quadrotor Trajectory Tracking Control in the Multiple Disturbances, *International Journal of Control, Automation and Systems*, 17(11), 2754–2768.

Mahony, R., Kumar, V., and Corke, P. (2012). Multirotor Aerial Vehicles: Modeling, Estimation, and Control of Quadrotor, *IEEE Robotics & Automation Magazine*, 19(3), 20-32.

Bouadi, H., Aoudjif, A., and Guenifi, M. (2015). Adaptive flight control for quadrotor UAV in the presence of external disturbances, *2015 6th International Conference on Modeling, Simulation, and Applied Optimization (ICMSAO)*, 1-6.

Bresciani, T. (2008). *Modelling, identification and control of a quadrotor helicopter*, MSc Thesis, Lund University, Sweden.

Da Silva Ferreira, M.A., Begazo, M.F.T., Lopes, G.C. (2020). Drone Reconfigurable Architecture (DRA): a Multipurpose Modular Architecture for Unmanned Aerial Vehicles (UAVs). *Journal of Intelligent and Robotic Systems,* 99, 517–534.

Dikmen, I.C., Arisoy, A., Temeltas, H. (2009). Attitude control of a quadrotor, *2009 4th International Conference on Recent Advances in Space Technologies*, 722-727.

Dong, W., Gu, G-Y., Zhu, X., Ding, H. (2015). Development of a Quadrotor Test Bed — Modelling, Parameter Identification, Controller Design and Trajectory Generation. *International Journal of Advanced Robotic Systems*.

Eltayeb, A., Rahmat, M.F., Basri, M.A.M. (2020). Sliding mode control design for the attitude and altitude of the quadrotor UAV, *International Journal on Smart Sensing and Intelligent Systems*, 13(1), 1-13.

Flores, G., González-Huitron, V., Rodríguez-Mata, A.E. (2020). Output Feedback Control for a Quadrotor Aircraft Using an Adaptive High Gain Observer, *International Journal of Control, Automation, and Systems*, 18(6), 1474–1486.

Gautam, D., Ha, C. (2013). Control of a Quadrotor Using a Smart Self-Tuning Fuzzy PID Controller. *International Journal of Advanced Robotic Systems*.

Jammazi, C. (2008). Backstepping and Partial Asymptotic Stabilization: Applications to Partial Attitude Control, *International Journal of Control, Automation, and Systems*, 6(6), 859-872.

Jeong, S.H., Jung, S. (2016). Cartesian space control of a quadrotor system based on low cost localization under a vision system, *International Journal of Control, Automation and Systems*, 14(2), 549–559.

Karahan, M., and Kasnakoglu, C. (2019). Modeling and Simulation of Quadrotor UAV Using PID Controller, *2019 11th International Conference on Electronics, Computers and Artificial Intelligence (ECAI)*, 1-4.

Lee, D., Joo, Y.H., Song, D. (2017). Local stability analysis of T-S fuzzy systems using second-order time derivative of the membership functions, *International Journal of Control, Automation and Systems*, 15(4), 1867–1876.

Meng, G.Z., Ma, K.M. (2020). Output Regulation for a Class of Uncertain Nonlinear Time-delay Systems by Output Feedback Control, International Journal of Control, Automation and Systems, 18(4), 867–876.

Oland, E., Andersen, T.S., Kristiansen, R. (2013). Underactuated Control of Quadrotors with collision Avoidance*, IFAC Proceedings*, 46(30), 162-167.

Pei, C., Zhang. J., Wang, X., Zhang, Q. (2018). Research of a non-linearity control algorithm for UAV target tracking

based on fuzzy logic systems, *Microsystem Technologies*, 24, 2237–2252.

Rui, W., Jinkun, L. (2017). Adaptive formation control of quadrotor unmanned aerial vehicles with bounded control thrust, *Chinese Journal of Aeronautics*, 30(2), 807-817.

Sanca, A.S., Alsina, P.J., and Cerqueira, J.d.J.F. (2008). Dynamic Modelling of a Quadrotor Aerial Vehicle with Nonlinear Inputs, *2008 IEEE Latin American Robotic Symposium*, 143-148.

Wang, P., Man, Z., Cao, Z., Zheng, J., and Zhao, Y. (2016). Dynamics modelling and linear control of quadcopter, *International Conference on Advanced Mechatronic Systems (ICAMechS)*, 498-503.

Wang, S., Zhang, J., Zhang, Q., Pei, C. (2017). An innovative fuzzy backstepping sliding mode controller for a Tri Rotor Unmanned Aerial Vehicle, *Microsystem Technologies*, 23, 5621–5630.

Vepa, R. (2016). *Nonlinear Control of Robots and Unmanned Aerial Vehicles: An Integrated Approach*, 531. CRC Press, Boca Raton, Florida.

Xiong, J., and Zhang, G. (2016). Sliding mode control for a quadrotor UAV with parameter uncertainties, *2016 2nd International Conference on Control, Automation and Robotics (ICCAR)*, 207-212.

Yigit Z. (2015). *Modeling and control of quadrotor unmanned aerial VTOL vehicle*, MSc Thesis, Istanbul Technical University, Turkey.

Zhao, J., Zhang, H., Li, X. (2020). Active disturbance rejection switching control of quadrotor based on robust differentiator, *Systems Science & Control Engineering*, 8(1), 605-617.

Zhou, L., Zhang, J., Houxin, S., Jin, H. (2019). Quadrotor UAV flight control via a novel saturation integral backstepping controller, *Automatika*, 60(2), 193-206.